Centralized, Distributed, and Module-Integrated Electric Power System Schemes in CubeSats: Performance Assessment

BAYAN HUSSEIN, (Graduate Student Member, IEEE),
AHMED M. MASSOUD, (Senior Member, IEEE),
AND TAMER KHATTAB, (Senior Member, IEEE)
Electrical Engineering Department, Qatar University, Doha, Qatar

Corresponding author: Bayan Hussein (bh1602414@qu.edu.qa)

ABSTRACT Pico-satellites, also called CubeSats, have gained significant attention in recent years because they offer a low-cost and low-power solution with low latency communication and high data rates compared to larger satellites. The most critical subsystem in a CubeSat is the Electrical Power Subsystem (EPS) that provides the needed power to operate the remaining subsystems. The EPS mainly incorporates solar panels (generation), power electronic converters (shaping and distribution), and battery cells (storage). One of the main factors in EPS design is the system's reliability. This work proposes a module-integrated (MI) scheme for EPS architectures to increase the reliability through modularity and redundancy. Furthermore, a comparison between different EPS architectures (centralized, distributed, and module-integrated EPS topologies) based on Direct Energy Transfer (DET) and Peak Power Transfer (PPT) is presented. A performance evaluation is conducted considering different factors, such as reliability, fault ride-through capability, efficiency, re-usability, and scalability. The results confirm that MI architectures have higher reliability than centralized and distributed architectures.

INDEX TERMS CubeSats, DC-DC converters, electric power system (EPS), low earth orbit (LEO) satellites, modularity, solar panels.

I. INTRODUCTION

CubeSats are small satellites built in a standard dimension of 1U ($10 \times 10 \times 10$ cm^3), weighing around 1.33 kg/U and can be extended to multiple units: 1U, 2U, 3U, and 6U [1]. They are deployed in the Low Earth Orbit (LEO) at altitudes less than 2000 km, with 90-120 minutes orbital period and 0-90° inclination angle [2]. They gained significant popularity within the last few years due to their lower cost, lower latency communication (0.02 seconds versus 0.5 seconds in geostationary satellites), and lower power consumption while providing wireless access with improved data rates [3]. The cubic structure (hence the name CubeSat) optimizes the surface area, thus enhancing solar power generation and thermal stability [4]. It also provides a standardized shape, enabling

batch launching as a secondary load to launching vehicles, significantly reducing launching costs.

The Electric Power Subsystem (EPS) is considered an essential subsystem of a CubeSat. This subsystem uses solar energy to generate the required power to operate the remaining subsystems in the CubeSat, including the communication system (COM), the attitude determination and control system (ADCS), the on-board computer (OBC), and the payload. As shown in Fig. 1, a general EPS includes power generation, power conditioning, power conversion, power storage, and power distribution modules [5]. Additionally, an EPS is equipped with protections for overcurrent, overvoltage, overcharge, and over-discharge [6]. The EPS design considers many factors, such as the altitude of the orbit, the mission and its duration, the arrangement and size of the photovoltaic (PV) panels, the high-speed movement of the CubeSat, the load profile, the weight, and volume restrictions [7].

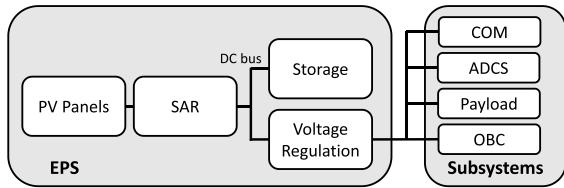The associate editor coordinating the review of this manuscript and approving it for publication was Snehal Gawande.

FIGURE 1. The general architecture of the subsystems in a CubeSat.

TABLE 1. Power budget in CubeSat subsystems [10].

Subsystem	Power Consumption (W)
COM (RX, TX)	4.4
ADCS	1.4
OBC	0.4
Payload	~1-2
EPS	0.16

The idea of integrating multiple functionalities into a single module for CubeSat designs goes beyond modules related to the same subsystem. For example, in [8] and [9], novel configurations were proposed for the design and integration of circularly polarized (CP) antennas on the surface of the PV panels to minimize the shadowing effect and maximize the absorbed solar radiation by the PV panels and as a result, maximize the power generation.

Since the EPS provides the power for the whole CubeSat, the design process requires knowledge of the power consumption of each subsystem in the CubeSat. Generally, the payload depends on the mission of the CubeSat. A general estimation for CubeSat's power budgeting is presented in Table 1 [10].

This work aims to present a review of the different EPS architectures based on Direct Energy Transfer (DET) and Peak-Power Transfer (PPT) with regulated, unregulated, and partially-regulated DC busses. Furthermore, we propose a new Module-Integrated (MI) scheme for EPS architectures to increase reliability and fault ride-through capabilities and reduce the failure probability of the EPS and mission. A reliability assessment of the different architectures confirms that MI schemes outperform conventional architectures.

This paper is organized as follows: in Section II, a general overview of the EPS components (generation, conditioning, storage, and distribution) is presented. Also, the literature review is conducted to identify the gaps. Section III discusses the specifications and ratings of CubeSat's components and modules. Section IV elaborates on the MI schemes and compares their reliability with conventional architectures. Then, Section V presents a discussion about the manufacturability of MI schemes. Lastly, Section VI concludes the paper.

II. EPS ARCHITECTURE AND CLASSIFICATION
A. POWER GENERATION
The primary source of electric power generation in a CubeSat is solar power. The PV panels are either attached to the faces

TABLE 2. Solar panel types available in CubeSat market.

Vendor	Product	Cell Type	Cell Efficiency
ACC Clyde Space [13]	Photon	3J (NeXt)	30.70%
Pumpkin [14]	Pumpkin Modular Solar Array System	3J (NeXt)	30.70%
	CubeSat Kit: Fixed Panels	3J (NeXt)	30.70%
Ecuadorian Space Agency [15]	EXA DMSA	Mono	19%
	EXA DMSA	3J (GaAs)	28%
DHV Technology [16]	DHV-CS-10	3J (GaAs)	30%
ISISPACE [17]	-	3J (GaAs)	30%
Azur Space [18]	4G32C-Advanced	4J (AlInGaP/AlInGaAs/ InGaAs/Ge)	32%
	3G30C-Advanced	3J (InGaP/GaAs/Ge)	30%
	S32	Mono	16.9%
	3G28C	3J (GaInP/GaAs/Ge)	28%
Blue Canyon Technologies [19]	-	3J	29.50%
GomSpace [20]	NanoPower	3J (GaInP/GaAs/Ge)	30%
Harris Corporation [21]	HSAT	3J (InGaP/GaAs/Ge)	-
Endursat [22]	-	3J	29.50%
NanoAvionics [23]	NanoAvionics GaAs	3J (GaInP/GaInAs/Ge)	29.50%

of the CubeSat, deployed in the wings, or both. The deployable panels are advantageous because they can be oriented in the direction of the Sun and harvest the maximum power [11], unlike the fixed panels. In [12], a multi-array lens system was proposed to increase the solar energy concentration on the PV panels for efficient power generation. The incidence angle, revolution, and rotation of the CubeSat were all considered. CubeSats generally may not receive the same irradiation amount in all positions along their orbits, resulting in eclipse conditions. Typically, the panels attached to opposite sides are connected in parallel because only one of them is exposed to solar irradiation at an instance [10].

The power generation can be affected by many factors, including temperature rise, weak illumination of the cell, distance from the Sun, and the CubeSat's orbital mechanics. Modeling of the orbit analytically and numerically using different techniques was discussed in [24]. In [25], an analytic model for the solar power of LEO satellites was developed considering the geometric representation of the orbit. The model considered the Keplerian elements that described the orbit with reference to the equator and the angle between the Sun radiations vector and the orbit plane. The incidence angle, eclipsing, and power values were calculated for an orbiting satellite. In [26], the characteristics of deployable solar panels and solar radiation torque were investigated using software algorithms to simulate different orbit scenarios. In [27], a simulation model for solar power generation

TABLE 3. EPS Systems configurations proposed in the literature.

	Contribution & Limitations	CubeSat / Mission	EPS Architecture	SAR (DET or MPPT)	No. of DC-DC converters	Harvested Power (W)	Efficiency
[32]	• DET in extreme low voltage cases (+) • Reliability was compromised at eclipse instances since the PV panels were incapable of feeding the system (-)	NutSat / Collect broadcast data from aircrafts with ADS-B sensor	Centralized	MPPT SEPIC/ Perturb & observe	4 SEPIC for MPPT, 3 Buck for loads Total: 7	19.457	Circuit efficiency: 85% MPPT tracking efficiency: 99%
[33]	• Modularized the PV panels and MPPT converters (+) • No modularization in the storage system (-)	Ten-Koh	Distributed	MPPT Boost/ N/A	N/A	10.98	Circuit efficiency: 88.49% MPPT tracking efficiency: 96%
[34]	• Modularized the PV panels and MPPT converters (+) • No modularization in the storage system (-)	N/A	Distributed	MPPT Buck/ Perturb & observe	4 Buck for MPPT 3 Regulators for loads Total: 7	75	Circuit efficiency: N/A MPPT tracking efficiency: 96.2%
[35]	• Modularized the PV panels and storage systems (+) • No MPPT operation to optimize power extraction (-)	N/A	Distributed	DET	N/A	4.76	Circuit efficiency: 99.5% MPPT Tracking efficiency: N/A
[36]	• A topology using half-bridges at the PV output terminals based on single inductors (+) • Half-bridges experience more switching and conduction losses and low efficiency (-)	1U Lab-based CubeSat	Centralized	MPPT Boost/ Perturb & observe	1 Boost for MPPT 3 Half Bridges 2 for loads Total: 6	2.25-3.1	Circuit efficiency: 95% MPPT Tracking efficiency: N/A
[37]	• EPS design considering latency & power requirements (+) • Analyzing the nadir orientation scenario only (-)	1U CubeSat for 5G Mission	Centralized	MPPT Boost/ Perturb & observe	N/A	20	Circuit efficiency: 92% MPPT Tracking efficiency: N/A

optimization is presented considering the PV array modeling, illumination level, calculation of the Sun's position, the orbital parameters, and the panel's generated power and energy. The total generated power is represented by [27],

$$P_{total} = \sum_{i=1}^{6} P_i \qquad (1)$$

where

$$P_i = S_0 \eta A \cos \gamma \qquad (2)$$

where S_0 is the solar index of the orbit, η and A are the efficiency and area of the PV panel, respectively, γ is the incident angle of the Sun with the PV panel, and $i = 1, 2, \ldots 6$ identifies the different faces of the CubeSat.

Multi-junction (MJ) solar cells are made up of many layers of materials that can efficiently absorb light and convert it into electrical energy. Triple-junction (TJ) PV panels (particularly GaInP/GaAs/Ge cells) are frequently used in the aerospace industry as they are significantly efficient for their cost compared to other cells and can absorb longer wavelength [28]. Modeling TJ solar cells through a detailed three-diode equivalent circuit based on the used materials in the TJ solar

panel was presented in [29]. A market overview is conducted in Table 2, showing the well-known CubeSat vendors and the associated PV panels they offer. Based on the CubeSat PV panels market study, around 87.5% of today's market is based on MJ panels whereas 12.5% use monocrystalline PV modules.

B. POWER CONDITIONING

The power conditioning unit delivers the voltage to the DC bus. However, the power produced from the PV panel depends on many environmental conditions. Even at the instances of maximum irradiance, the mismatch in the load can cause the extracted power from the PV panels to drop. The maximum possible power is generated from a solar panel when the load impedance matches the panel's internal resistance, calculated from the panel's I-V curve. To mitigate this issue, Solar Array Regulators (SARs) are inserted after the PV Panel. SARs are required for two main tasks: load matching and prevention of batteries' overcharging. They generally have two approaches, Direct Energy Transfer (DET) and Peak-Power-Transfer (PPT). In DET-based topologies, the energy is transferred directly through the diodes that connect

TABLE 4. Literature works that conducting comparative assessments of EPS architectures.

|	[38]	[39]	[41]	[42]	Proposed
Publication Year	2011	2013	2021	2021	2022
Contribution	Comparison of architectures	Comparison of architectures	Comparison of architectures	Extensive comparison of architectures	Proposing module-integrated (MI) concept in EPS + Comparison of architectures
Comparison Metrics	Reliability	- Efficiency - Reliability - Cost	- Orbital Efficiency - Battery Sizing - Component Count - Reliability	- Component Count - Efficiency	Reliability
Compared Architectures and their number, N	PPT/DET + Regulation Method	PPT/DET/Hybrid + Regulation Method	PPT + Regulation Method	PPT/DET/Hybrid + Regulation Method + Conversion Stages + Location of converters	Centralized/decentralized/MI + PPT/DET/Hybrid + Regulation Method
	N=8	N=10	N=6	N=17	N=21
Used Techniques	Failure Mode and Effect Analysis (FMEA)	Series/Parallel Connection	Single-point-of-failure (SPOF)	Qualitative Discussion	- Series/Parallel Connection - Single-point-of-failure (SPOF)
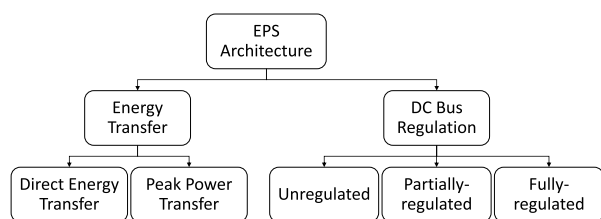
FIGURE 2. Classification of EPS architectures.

the panel to the DC bus. A parallel regulator can be added to bypass the extra power when batteries are fully charged. The load dictates the operating point of the panel, which may not be the maximum power point [30]. In contrast, PPT-based topologies have a series-connected DC-DC converter between the panel and the bus. This unit sets the operating point of the PV panel such that the load is matched to the characteristic resistance of the panel to draw the maximum power. PPT topologies include fixed-power-point-tracking (FPPT) and maximum-power-point-tracking (MPPT). The isolation provided by the DC-DC converter in MPPT-based topologies allows the connection of multiple PV panels to a single DC bus. Mostly, MPPT topologies are preferred for CubeSats to maximize power harvesting. In [31], a combination of DET and PPT concepts was proposed, where DET-based PV panels fed Lithium-ion (Li-ion) batteries, and PPT-based PV panels fed supercapacitors.

Generally, the categorization of EPS architectures, as illustrated in Fig. 2, can be in terms of the energy transfer method (DET or PPT) or the voltage regulation of the DC bus, where it can be unregulated, partially-regulated or fully regulated. The unit, or the lack thereof, interfacing the DC bus and the load dictates the topology.

C. STORAGE SYSTEM

The significance of an energy storage system is for cases where the power from the source is unavailable or insufficient, like eclipse cases or increased data rate requirements cases, respectively. The storage system, typically rechargeable batteries, can be connected to the DC bus either directly or via a power electronic unit that acts as a battery charger regulation (BCR) or a voltage regulator (VR). When the storage system is connected to the bus directly, the bus is unregulated. In regulated DC bus topologies, the storage units are connected through a BCR or a VR, both of which stabilize the bus voltage at a pre-defined value. Generally, loads in the CubeSat can be source-fed, battery-fed, or both. That is, if the power generation does not meet the load demand, the storage system provides the needed power. Otherwise, the excess power is stored in the storage system. Li-ion batteries are commonly used in CubeSats because of their ability to withstand intensive radiation. They are characterized by high energy density (>120 Wh/kg) and a long life-cycle [32]. However, due to the charging and discharging performances of the on-board Li-ion cell, high heat is dissipated, negatively affecting its life cycle and causing complications in the thermal management of the system. Supercapacitors or ultracapacitors (SC or UC, respectively) have been introduced recently in the design of CubeSats due to their broader operating temperature range and extremely high life cycle. Combining the Li-ion and supercapacitor technologies can result in a system that meets the requirements with increased reliability and performance [33].

## D. VOLTAGE REGULATION AND POWER DISTRIBUTION

DC-DC converters are employed to regulate the voltage levels from the DC bus to the required voltage levels for the
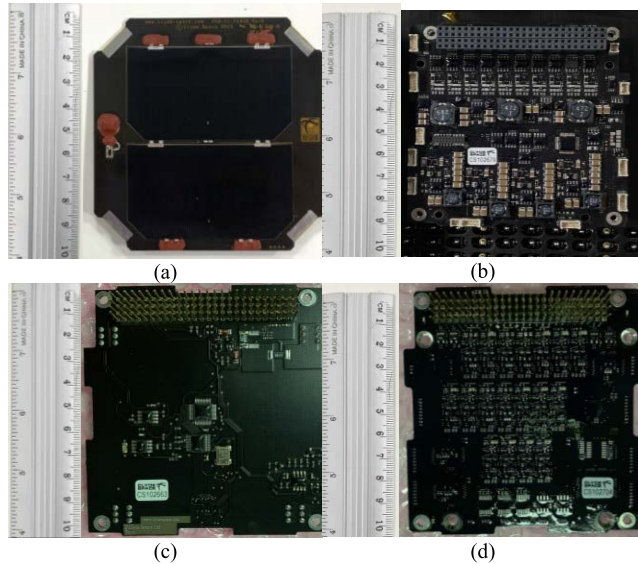
FIGURE 3. Clyde Space CubeSat modules (a) two-cell solar panel (b) EPS module (c) Battery module (d) PDM.

FIGURE 4. Illustration of module-integrated EPS in a CubeSat.

remaining subsystems. The power distribution system allocates the power to CubeSat's remaining subsystems through the Power Distribution Module (PDM) that consists of multiple switches rated at different voltages to deliver power to the loads.

Table 3 summarizes the recent works proposing and developing novel EPS for CubeSat [34]–[39]. The table organizes them based on the contribution of the work, the mission of the CubeSat, the architecture of the EPS, the employed SAR technique, the used DC-DC converter, and the employed algorithm for PPT-based architectures. While some contributions in the literature presented details about proposed EPS, other contributions included comparisons between different EPS architectures for performance evaluation, as summarized in Table 4. In [40], an approach to estimate the reliability of DET and PPT-based EPS was presented, considering the EPS elements' redundancy. DET architectures were found to be more reliable than the PPT-based ones. In [41], ten different DET- and PPT-based topologies with different DC bus regulation methods were compared in terms of reliability, efficiency, and cost-effectiveness. Among ten topologies, it was found that semi-regulated DET-based EPS architecture has the highest performance. In [42], the authors compared the efficiency of four different architectures, where the prime difference was the interfacing unit between the panel and DC bus. They concluded that the very-low-drop-out (VLDO) architecture had the highest efficiency but not the maximum harvested energy. In [43], the work focused on PPT-based architectures with different DC bus regulation methods. The comparison concluded that unregulated voltage regulation has an optimal performance in terms of reliability, number of components, battery sizing, and orbital efficiency. In [44], a comprehensive review of seventeen different DET and PPT architectures was presented. The classification of the
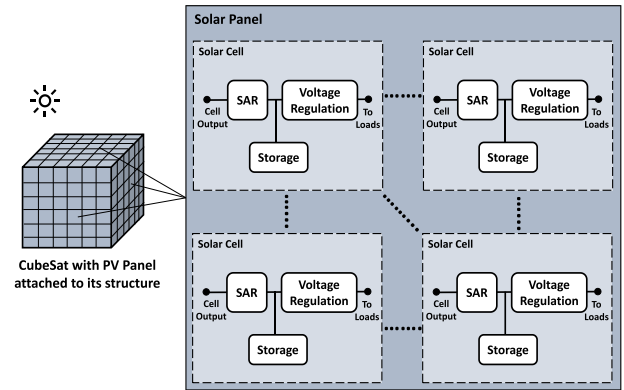
architecture was in terms of four different categories: the regulation of the DC bus, the number of conversion stages, the energy transfer method, and the location of the DC-DC converter. The review concluded that DET-based architectures with unregulated bus had the least number of components, which consequently enhanced the overall efficiency of the EPS.

However, among the literature that discussed modularity, none has considered modularity in the overall design of the EPS, which can further boost the reliability of the EPS. Thus, the contribution of this work can be highlighted as:

1- Since the success or failure of CubeSat's mission depends solely on the EPS performance, a modified Module-Integrated (MI) scheme for the EPS is required, where the EPS is integrated into the back of the PV panel. MI architectures mainly enhance reliability by increasing the redundancy of the elements. It allows designing smaller modules at low-power levels and utilizing them in a plug-and-play approach, making it easier to reduce or alleviate power levels based on the mission requirements. MI EPS architectures offer redundancy, re-usability, scalability, and reduction of development time.

2- To evaluate the performance, a comparison is carried out between MI and centralized EPS architectures. The comparison of EPS architecture should consider the size and component count of the system, the overall efficiency, reliability, scalability, and re-usability of the EPS.

III. CubeSat SPECIFICATIONS

CubeSats are comprised of different modules, including PV panels, EPS module, battery module, and PDM, as shown in Fig. 3. They have maximum ratings of 0.89 W power, 196 mA current, and 4.5 V voltage. The open-circuit voltage is 5.178 V, whereas the short-circuit current is 0.205 A. The output of the two-cell solar panel is connected to the EPS module shown in Fig. 3(b) through four BCRs. All BCRs have 10 V input voltage and 750 mA input current. The EPS can operate at temperatures −40 °C to 85 °C and has
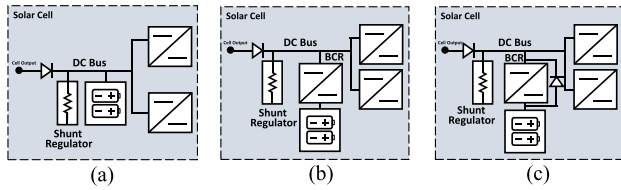
FIGURE 5. Module-integrated DET-based architectures (a) Arch-1: MI DET unregulated DC-bus and floating battery (b) Arch-2: MI DET regulated DC-bus (c) Arch-3: MI DET sun-regulated DC-bus.
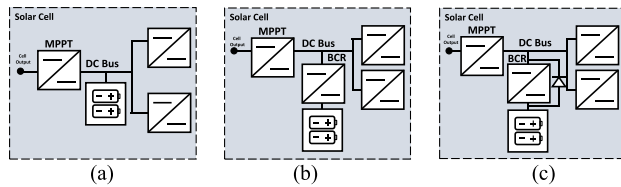

FIGURE 6. Module-integrated PPT-based (a) Arch-4: MI PPT unregulated DC-bus (b) Arch-5: MI PPT unregulated DC-bus (c) Arch-6: MI PPT sun-regulated DC-bus.

three busses: 3.3 V, 5 V, and 12 V. The maximum output current for each is 4.5 A, 4.5 A, and 1.5 A, respectively. The output of the BCR is connected to the DC bus, which has a Lithium polymer battery connected to it. The battery module shown in Fig. 3(c), has maximum and minimum voltages of 8.27 V and 6.2 V, respectively. The maximum output current from the battery bus is 4.5 A at voltages of 8.26 V. Lastly, the PDM in Fig. 3(d) has 13 switches to distribute the voltage to the loads. The ratings of the switches are distinguishable at 3.3 V, 5 V, 12 V, and 8.3 V for the battery voltage. The PDM is equipped with overcurrent protection and an I^2C communication node at 0×50 address and 10 MHz operating frequency to access all telemetry on the switchboard.

IV. MODULE-INTEGRATED SCHEMES

Modularity in the EPS design can be added on different levels. In this work, redundancy is added to the architecture at a cell level, and the concept can then be extended to a group-of-cells level. The proposed idea is to modularize all components of the EPS–including the DC-DC converters and battery storage system– and integrate each module at the back of the solar cell, as illustrated in Fig. 4. Instead of having the EPS occupying the limited space inside the CubeSat, the integration within the PV panel will provide more spatial area to add mission-related components while complying with the weight and volume restrictions. Module-integrated (MI) schemes allow the development and optimization of minimized EPS within a single solar cell for a given power level. Then, a plug-and-play approach can be employed to control the total generated power level from the solar panel, based on the requirements. The merits of this design can be stated as the following:

1- The system's reliability and fault ride-through capabilities are increased because of modularity. A failure of a
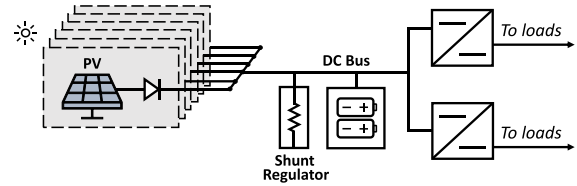
FIGURE 7. Arch-7: DET-based unregulated DC-bus.
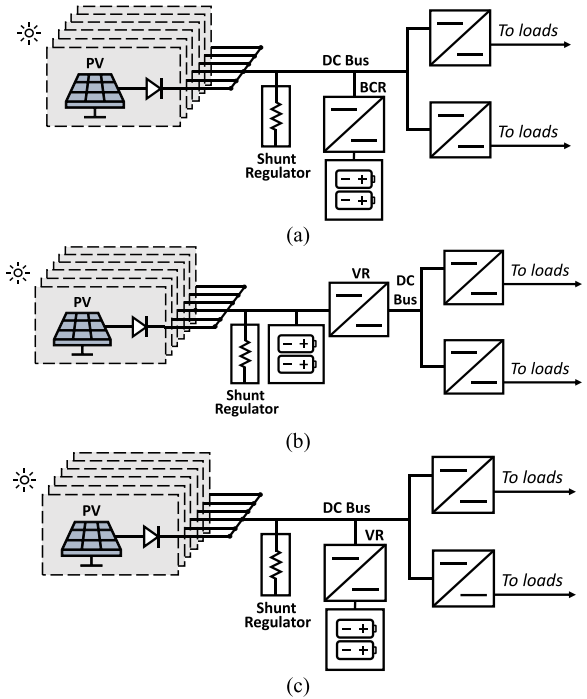
FIGURE 8. DET-based regulated DC-bus (a) Arch-8: DET regulated with BCR (b) Arch-9: DET regulated with series VR (c) Arch-10: DET regulated with VR.

single cell or a single EPS component does not severely impact the operation of the satellite as other modules will override it.

2- The scalability of the system is increased because of the plug-and-play approach. The total power generated by the EPS can be changed based on the used number of cells in the PV panel.

3- The fabrication and development time is reduced because re-sizing the elements (including DC-DC converters and battery storage systems) for a given power level is not an issue.

A. MI EPS TOPOLOGIES

The modularity aspect can be added to the EPS design at a cell level or a group-of-cells level. Either way, the reliability is increased. Based on the MI concept, both DET and PPT architectures with different voltage regulation methods are analyzed. This section studies cell-modularized MI EPS schemes. MI DET-based architectures with different voltage regulation methods are shown in Fig. 5. The architecture
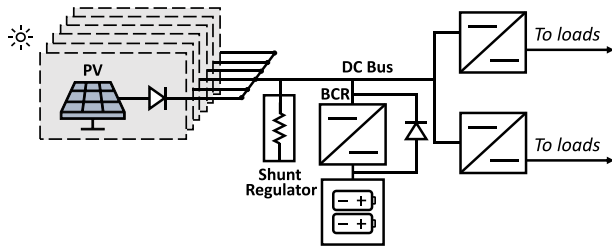
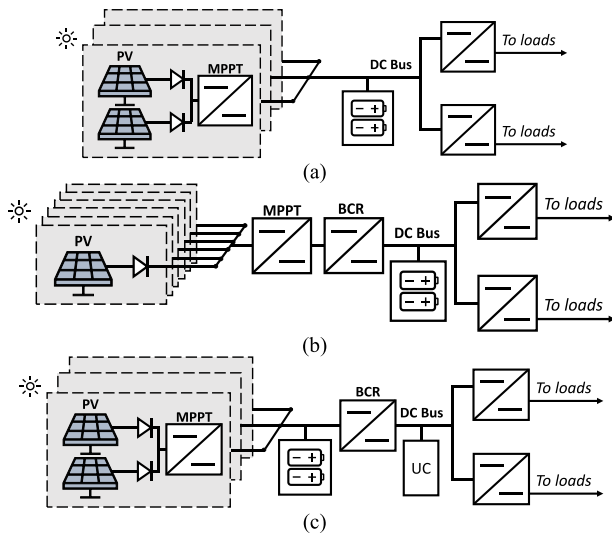**FIGURE 9.** Arch-11: DET-based sun-regulated DC-bus.

FIGURE 10. PPT-based unregulated DC-bus (a) Arch-12: PPT unregulated DC-bus (b) Arch-13: PPT unregulated DC-bus with series-BCR (c) Arch-14: PPT unregulated DC-bus with floating battery and ultra-capacitor.

presented in Fig. 5(a) is simplistic and has a low component count. Despite having high efficiency, connecting the battery unit directly to the DC bus is not a recommended practice since the operating point of the solar cell will be fixed, and thus the maximum power cannot be extracted. In Fig. 5(b), a BCR is added between the battery and the bus to control the battery voltage and current through multi-loop control. Fig. 5(c) shows the architecture for a MI DET-based sun-regulated DC bus. The BCR regulates the battery voltage and current throughout the sunlit instances and is disabled during eclipse, where the battery supplies the load with the required demand. MI PPT-based architectures with different voltage regulations are illustrated in Fig. 6. The MPPT unit in these architectures extracts the maximum power from the solar panel and provides it to the DC bus. In Fig. 6(a), the battery is floating, whereas, in Fig. 6(b), it is interfaced with a BCR. In Fig. 6(a), the MPPT operates as VR when the battery is fully charged. Fig. 6(c) shows the sun-regulated PPT-based architecture, where the BCR regulates the battery charging process in sunlit instances and gets disabled during eclipse periods. The architecture in Fig. 6(c) offers flexibility in battery sizing because the BCR unit regulates the bus voltage based on the battery voltage.

B. COMPARISON WITH EXISTING ARCHITECTURES

This section discusses architectures with different energy transfer methods (DET and PPT) using unregulated, fully-regulated, and partially-regulated DC buses.

1) DET-BASED ARCHITECTURES

The architectures shown in Fig. 7-9 are all DET-based architectures. In Fig. 7, the DC bus is unregulated, where the panel's voltage is dedicated by the battery voltage, and the current of the PV panel depends on its I-V curve. This means that the PV may be operating at a point other than the MPP. During eclipse periods, the battery feeds the loads. Fig. 8 presents DET-based architectures with a regulated bus. In Fig. 8(a), a BCR is added before the battery to control the charging current. In Fig. 8(b), the DC bus is regulated by a VR unit connected in series with the load converters. Arch-7 and Arch-8 have more component count and thus experience more losses. In Fig. 8(c), the VR is connected to the battery rather than the load-side converters to balance the power between the generation side and the load demand [33].

In Fig. 9, the DET sun-regulated EPS is shown. During the sunlit periods, the BCR operates and regulates the charging process. During the eclipse instances, the BCR is blocked, and the battery supplies the load through the diode only, reducing the conversion losses compared to the previous architectures employing BCR units.

2) PPT-BASED ARCHITECTURES

Most CubeSats employ PPT-based architectures to retrieve the maximum power from the Sun [32]. Fig. 10-12 present architectures that employ MPPTs with different regulation methods for the DC bus. In Fig. 10, PPT-based unregulated bus schemes are illustrated. In Fig. 10(a), each group of panels is connected to a designated MPPT unit so that each group extracts its maximum power based on its irradiation levels. The DC bus is kept unregulated by connecting the battery directly to the DC bus. However, unlike DET-based unregulated architecture, the MPPT unit is controlled to optimize power extraction of the PV panel regardless of the output voltage. Thus, the battery no longer dictates the operating point of the PV. In this architecture, the MPPT unit operates like a VR if the battery voltage is at its peak to maintain that level, and the PV panel supplies the load. In Fig. 10(b), parallel-connected panels are interfaced with the remaining EPS through a single unit of MPPT. Although this reduces the component count, it degrades the overall performance because it assumes that all PV panels are exposed to the same irradiation level, which may not be the case. In Fig. 10(c), a hybrid storage system is employed using Ultra-Capacitors (UC) in addition to the typical battery pack to increase efficiency and reliability [34]. A regulator for battery discharge is added between the two units to control the current from the battery to the loads and UC.

TABLE 5. SPOF analysis for EPS architectures.

|	SR	MPPT	BCR	Battery	VR	DC/DC	Total		SR	MPPT	BCR	Battery	VR	DC/DC	Total
Arch-1							0	Arch-12	-	No	-	Yes	-	Yes	2
Arch-2							0	Arch-13	-	Yes	Yes	Yes	-	Yes	4
Arch-3							0	Arch-14	-	No	Yes	Yes	-	Yes	3
Arch-4		Due to redundancy, there are no SPOF in MI architectures					0	Arch-15	-	No	-	Yes	Yes	Yes	3
Arch-5							0	Arch-16	-	No	Yes*	Yes	-	Yes	3
Arch-6							0	Arch-17	-	Yes	-	Yes	Yes	Yes	4
Arch-7	No	-	-	Yes	-	Yes	2	Arch-18	-	No	-	Yes	No	Yes	2
Arch-8	No	-	Yes	Yes	-	Yes	3	Arch-19	-	No	-	Yes	Yes	Yes	3
Arch-9	No	-	-	Yes	Yes	Yes	3	Arch-20	-	Yes	-	Yes	-	Yes	3
Arch-10	No	-	-	Yes	Yes	Yes	3	Arch-21	-	Yes	-	Yes	-	Yes	3
Arch-11	No	-	Yes	Yes	-	Yes	3				*The BCR in Arch-16 acts like BCR and VR units			
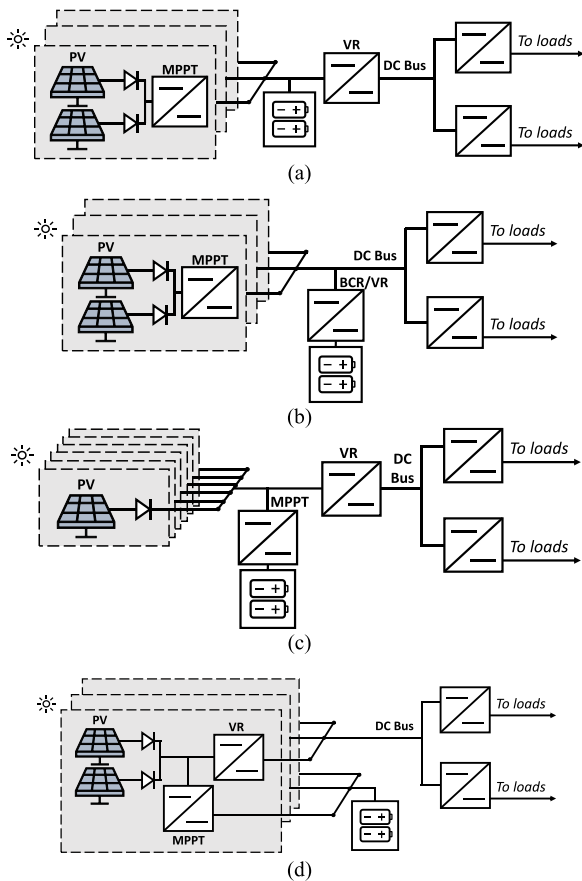
FIGURE 11. PPT-based regulated DC-bus (a) Arch-15: PPT regulated DC-bus with series VR (b) Arch-16: PPT regulated DC-bus with parallel BCR/VR (c) Arch-17: PPT regulated DC-bus with series VR and parallel MPPT (d) Arch-18: PPT regulated DC-bus with modular series VR and parallel MPPT.

FIGURE 12. Arch-19: PPT-based sun-regulated DC-bus.
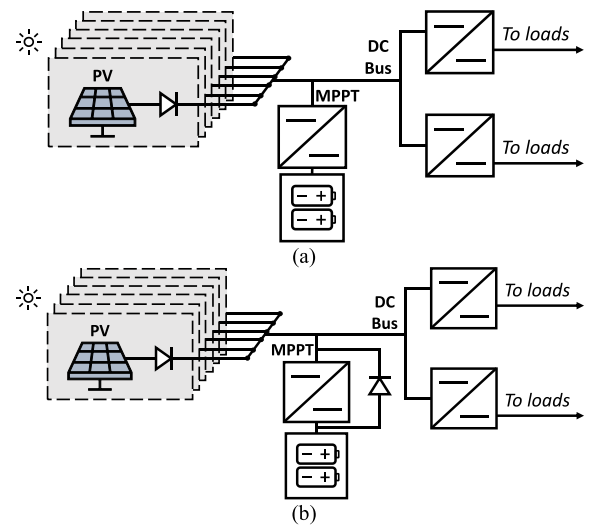
FIGURE 13. Hybrid architecture (a) Arch-20: hybrid unregulated (b) Arch-21: hybrid sun-regulated.

In Fig. 11, PPT-based regulated DC bus EPS is presented. In Fig. 11(a), a VR unit is added before the load converters to keep the voltage of the bus at a pre-defined value. In Fig. 11(b), the topology allows a wide range of battery
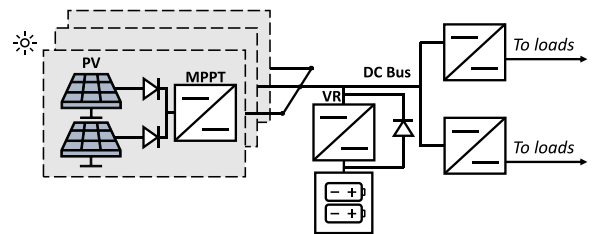
choices because the DC-DC converter unit can operate as a BCR or a VR. This, with the MPPT unit, allows using higher voltages at DC bus and hence reduce the conduction losses. In Fig. 11(c), MPPT and VR units are connected to the output of the parallel-connected panels. In Fig. 11(d), a parallel MPPT unit is connected to each group to maximize power generation from the PV panel. This output is fed to a
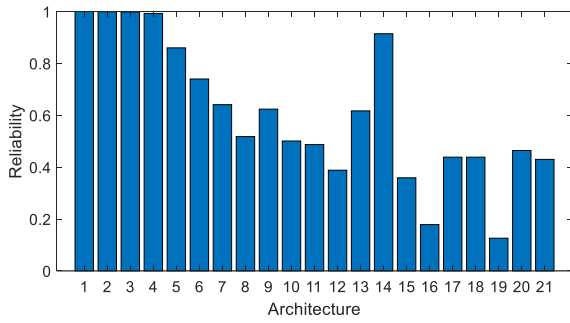
FIGURE 14. Bar chart of the reliability of each architecture based on the series/parallel connection of individual units.

TABLE 6. Comparison between centralized, distributed, and MI EPS.

	Centralized	Distributed	MI
Organization	Single unit combining all components	Multiple units, each combining related components	Cells are integrated with their PEC and batteries
Component Count	Low	Medium	High
Occupied Volume	Large	Medium	Small
Efficiency	High	High	Highest
Reliability	Low	Medium	High
Cost	Low	Medium	High

VR unit to regulate the DC bus. In Fig. 12, a sun-regulated PPT-based architecture is shown. The VR unit maintains the voltage of the DC bus during the sunlit period and gets blocked by the diode during the eclipse. At fully charged batteries, the VR is blocked, and the MPPT maintains the bus voltage. In Fig. 13, DET-and-PPT hybrid architectures are illustrated. In Fig. 13(a), the MPPT unit ensures maximum power extraction. When the battery's voltage is at its maximum, the architecture becomes like the DET-based regulated bus architecture, where the bus is regulated at maximum voltage battery. In Fig. 13(b), a similar scheme is presented with a diode added parallel with the MPPT unit. This allows the MPPT unit to operate during sunlit periods and maintains the voltage of the bus at the battery's peak. During the eclipse, the battery discharges through the diode to feed the loads, and the MPPT is disabled. In this topology, the maximum battery voltage should be lower than the PV's MPP to avoid diode conduction during sunlit periods.

C. RELIABILITY CALCULATIONS

The reliability of the EPS is of utmost importance. Thus, redundancy is ensured in MI-EPS architectures to improve the system's reliability. To further study and assess the reliability of each architecture, this section considers two techniques: the single-point-of-failure (SPOF) and the series/parallel connection of the components.

1) SINGLE-POINT-OF-FAILURE (SPOF)

SPOF are points in an architecture that, if failed, would cause the complete system to fail. Architectures with the least number of SPOF are considered the most reliable. In Table 5, a SPOF analysis is given for each architecture. It should be noted that module-integrated architectures do not have any SPOF because of the components' redundancy and fault ride-through capabilities. The results show that they are considered the most reliable architectures among all of them. In the SPOF analysis, the shunt regulators (SR) are not considered SPOF since they are connected in parallel with the PV panels, and their failure does not stop supplying the energy to the load. A single MPPT is not considered a SPOF because the

remaining MPPT units can still supply energy to the loads. However, in architectures 13 and 17, MPPT is considered a SPOF because it is a single unit rather than a modularized one. Furthermore, both the BCR and the battery are considered SPOF because the first failure will cause the energy storage system to be disconnected from the loads, whereas the second failure would stop the mission immediately if the panels are not supplying sufficient power. The VR units are considered SPOF only if they disconnect the loads or the battery from the panels. Lastly, the DC-DC converters on the load side are all considered as SPOF as they disconnect the load from both sources of energy: the PV panels and the battery. The results of this method confirm that MI architectures have higher reliabilities than the others due to redundancy and no SPOFs.

2) SERIES/PARALLEL CONNECTION

In this method, the overall reliability of each architecture considers the series or parallel connection of the unit. Given the reliability of the two units, R_1 and R_2, the reliability of their series connection is calculated through [23]

$$R_s = R_1 R_2 \tag{3}$$

whereas the reliability of their parallel connection is calculated through [23]

$$R_p = 1 - (1 - R_1)(1 - R_2) \tag{4}$$

Following this convention, the overall reliability of each architecture is calculated, and the bar chart in Fig. 14 summarizes the calculations and confirms that MI architectures are the most reliable among the 21 discussed architectures. It is also noticed that Arch-14 has high reliability due to the UC employed along with the battery storage system. In general, DET-based architectures are more reliable than PPT architectures, but this comes with the cost of losing the MPPT operation. A compromise is to employ MPPT in MI architectures to have higher reliability and a better power extraction scheme.

V. DISCUSSION

Recent reported EPS in the literature could be classified into centralized EPS architectures or distributed EPS architectures. This work proposes a new scheme for EPS architectures, module-integrated EPS architectures. A comparison is conducted between the centralized, distributed, and module-integrated (MI) architectures in terms of the architecture organization, the component count, the occupied volume, the anticipated efficiency, and the reliability. The results are shown in Table 6. Centralized EPS architectures have all components connected to a central unit summoning all power electronic converters (PEC) and a common DC bus that feeds the respective loads. These architectures are simple, size-efficient, and inexpensive, but they have low reliability because a single fault can destruct the whole system, consequently affecting the mission of the CubeSat. In contrast, each PEC is placed with its respective component in distributed EPS architectures. The MPPT converter is placed near the PV panel, the BCR is placed near the battery, and the DC-DC converter is placed near the loads, each in a distributed manner on separate units. These architectures have increased reliability due to redundancy. They are also characterized by re-usability and reduced noise levels due to placing each PEC near its subsystem. Lastly, module-integrated architectures work by cell-level modularity, where each solar cell has its own PEC and storage cells attached at the back. The EPS is designed such that the overall power is divided into modules. This allows employing components with lower ratings, further reducing the EPS size and giving room for other subsystems in the CubeSat. Although the component count and the cost are increased, these architectures have increased reliability compared to the others, which is confirmed in the previous section using two techniques. Moreover, MI architectures achieve scalability and allow a plug-and-play approach to alleviating power levels as needed. They have increased performance in addition to reduced development time. The performance is enhanced because each cell has its own PEC instead of a single MPPT for many cells with different characteristics and temperatures. As identical modules are fabricated, the time associated with EPS development is reduced because the testing and verification processes are conducted once. Furthermore, using low-power rated components reduces the overall cost.

The manufacturing process of module-integrated architectures includes manufacturing integrated solar panels with PEC attached to their back. This will also reduce the weight and size of the EPS since smaller components are employed. To discuss the manufacturability of module-integrated architectures, the modular-integration concept is further divided into two designs:

- Semi-module-integrated, where the components of the EPS are all modularized, but batteries are centralized. These architectures are similar to distributed EPS architectures, but the modularity is implemented at a cell level, and the EPS components are integrated at the back of the cell itself.
- Fully module-integrated, where the components of the EPS are all modularized, including the batteries.

In semi-module-integrated architectures, the reliability of the overall system is compromised (because the battery is centralized rather than distributed) with the manufacturability.

Typical batteries can be employed with specific energy and voltage ratings for the EPS design. On the other hand, fully module-integrated architectures require manufacturing special batteries that have to be smaller to fit the cell with the remaining PEC, complicating the manufacturing process. Furthermore, the testing process is simpler for semi-module-integrated because an experimental prototype can readily be constructed with commercial off-the-shelf (COTS) batteries.

To sum up, semi-module-integrated architectures have higher reliability than distributed and centralized architectures, and it is more feasible and manufacturable than fully-module-integrated architectures.

VI. CONCLUSION

In this work, a performance assessment has been conducted between different EPS architectures, namely the centralized, distributed, and MI architectures. The main advantage of MI architectures is the added redundancy, which further improves the reliability of the EPS. Two main categories were reviewed: DET and PPT architectures. Unregulated, regulated, and sun-regulated methods were investigated. The concept of MI was extended to these architectures, and a comparison in terms of reliability was conducted. The two techniques (SPOF and series/parallel connection) used to study the reliability confirmed that MI architectures are highly reliable. Among MI architectures, DET-based EPS had higher reliability. In addition to that, MI architecture offers a plug-and-play approach where the overall power of the EPS can be changed according to the needs of the CubeSat. This, in turn, is expected to reduce the development time and cost and simplify the production process. MI architectures essentially offer scalability, re-usability, and high reliability. MI architectures can be further divided into semi-module-integrated and fully-module-integrated architectures. The main difference between these two is the connection of the battery storage system: centralized for the first and distributed for the second. The impact of this differentiation is mainly in the testing and manufacturing processes, where semi-module-integrated architectures allow employing typical COTS batteries instead of manufacturing special batteries with particular specifications

REFERENCES

[1] I. U. Zaman, A. Eltawil, and O. Boyraz, "Wireless communication technologies in omnidirectional CubeSat crosslink: Feasibility study and performance analysis," *IEEE J. Miniaturization Air Space Syst.*, vol. 2, no. 3, pp. 157–166, Sep. 2021.

[2] M. R. Patel, *Spacecraft Power Systems*. Boca Raton, FL, USA: CBC Press, 2005.

[3] L. You, K.-X. Li, J. Wang, X. Gao, X.-G. Xia, and B. Ottersten, "Massive MIMO transmission for LEO satellite communications," *IEEE J. Sel. Areas Commun.*, vol. 38, no. 8, pp. 1851–1865, Aug. 2020.

[4] N. Saeed, A. Elzanaty, H. Almorad, H. Dahrouj, T. Y. Al-Naffouri, and M.-S. Alouini, "CubeSat communications: Recent advances and future challenges," *IEEE Commun. Surveys Tuts.*, vol. 22, no. 3, pp. 1839–1862, 3rd Quart., 2020.

[5] A. Ali, M. R. Mughal, H. Ali, and L. Reyneri, "Innovative power management, attitude determination and control tile for CubeSat standard NanoSatellites," *Acta Astronautica*, vol. 96, pp. 116–127, Mar. 2014.

[6] M. I. Desai, F. Allegrini, R. W. Ebert, K. Ogasawara, M. E. Epperly, D. E. George, E. R. Christian, S. G. Kanekal, N. Murphy, and B. Randol, "The CubeSat mission to study particles," *IEEE Aerosp. Electron. Syst. Mag.*, vol. 34, no. 4, pp. 16–28, Apr. 2019.

[7] O. Khan, M. E. Moursi, H. Zeineldin, V. Khadkikar, and M. Al Hosani, "Comprehensive design and control methodology for DC-powered satellite electrical subsystem based on PV and battery," *IET Renew. Power Gener.*, vol. 14, no. 12, pp. 2202–2210, Sep. 2020.

[8] S. K. Podilchak, D. Comite, B. K. Montgomery, Y. Li, V. G.-G. Buendia, and Y. M. M. Antar, "Solar-panel integrated circularly polarized meshed patch for CubeSats and other small satellites," *IEEE Access*, vol. 7, pp. 96560–96566, 2019.

[9] S. Zarbakhsh, M. Akbari, M. Farahani, A. Ghayekhloo, T. A. Denidni, and A. R. Sebak, "Optically transparent subarray antenna based on solar panel for CubeSat application," *IEEE Trans. Antennas Propag.*, vol. 68, no. 1, pp. 319–328, Jan. 2020.

[10] S. Acharya, F. Alshehhi, A. Tsoupos, O. Khan, M. Elmoursi, V. Khadkikar, H. Zeineldin, and M. Al Hosani, "Modeling and design of electrical power subsystem for CubeSats," in *Proc. Int. Conf. Smart Energy Syst. Technol. (SEST)*, Sep. 2019, pp. 1–6.

[11] F. Santoni, F. Piergentili, G. P. Candini, M. Perelli, A. Negri, and M. Marino, "An orientable solar panel system for nanospacecraft," *Acta Astronautica*, vol. 101, pp. 120–128, Aug. 2014.

[12] H.-U. Oh and T. Park, "Experimental feasibility study of concentrating photovoltaic power system for CubeSat applications," *IEEE Trans. Aerosp. Electron. Syst.*, vol. 51, no. 3, pp. 1942–1949, Jul. 2015.

[13] AAC Clyde Space. *Solar Arrays*. Accessed: Apr. 19, 2022. [Online]. Available: https://www.aac-clyde.space/what-we-do/space-products-components/photon-solar-arrays

[14] Pumpkin Space Systems. *CubeSat Kit Standard Solar Panels*. Accessed: Apr. 19, 2022. [Online]. Available: https://www.pumpkinspace.com/store/c25/CubeSat_Kit%E2%84%A2_Standard_Solar_Panels.html

[15] *Ecuadorian Space Agency (EXA) | Satsearch*. Accessed: Apr. 19, 2022. [Online]. Available: https://satsearch.co/suppliers/exa

[16] DHV Technology. *Products*. Accessed: Apr. 19, 2022. [Online]. Available: https://dhvtechnology.com/products/

[17] ISISPACE. *Small Satellite Solar Panels*. Accessed: Apr. 19, 2022. [Online]. Available: https://www.isispace.nl/product/isis-cubesat-solar-panels/

[18] Azur Space. *Space Solar Cells*. Accessed: Apr. 19, 2022. [Online]. Available: http://www.azurspace.com/index.php/en/products/products-space/space-solar-cells

[19] Blue Canyon Technologies. *Components*. Accessed: Apr. 19, 2022. [Online]. Available: https://bluecanyontech.com/components

[20] GomSpace. *NanoPower DSP*. Accessed: Apr. 19, 2022. [Online]. Available: https://gomspace.com/shop/subsystems/power/nanopower-dsp.aspx

[21] S. T. Gillespie, *HSAT-1*. Melbourne, FL, USA: Harris Corporation, 2016.

[22] Endursat. *Power in Space*. Accessed: Apr. 19, 2022. [Online]. Available: https://www.endurosat.com/cubesat-store/cubesat-solar-panels/3u-solar-panel-xy/

[23] NanoAvionics. *CubeSat GaAs Solar Panel*. Accessed: Apr. 19, 2022. [Online]. Available: https://nanoavionics.com/cubesat-components/cubesat-gaas-solar-panel/

[24] W. Ley, K. Wittmann, and W. Hallmann, Eds., *Handbook of Space Technology*. Hoboken, NJ, USA: Wiley, 2009.

[25] J. P. Grey, I. R. Mann, M. D. Fleischauer, and D. G. Elliott, "Analytic model for low Earth orbit satellite solar power," *IEEE Trans. Aerosp. Electron. Syst.*, vol. 56, no. 5, pp. 3349–3359, Oct. 2020.

[26] S. A. Ibrahim and E. Yamaguchi, "Comparison of solar radiation torque and power generation of deplotable solar panel configurations on nanosatellites," *Aerospace*, vol. 6, no. 50, pp. 1–22, 2019.

[27] D. Y. Lee, J. W. Cutler, J. Mancewicz, and A. J. Ridley, "Maximizing photovoltaic power generation of a space-dart configured satellite," *Acta Astronautica*, vol. 111, pp. 283–299, Jun. 2015.

[28] Y. Kovo, *State of the Art of Small Spacecraft Technology*. Washington, DC, USA: NASA, 2020.

[29] A. B. Hussain, A. S. Abdalla, A. S. Mukhtar, M. Elamin, R. Alammari, and A. Iqbal, "Modelling and simulation of single- and triple-junction solar cells using MATLAB/SIMULINK," *Int. J. Ambient Energy*, vol. 38, no. 6, pp. 613–621, Aug. 2017.

[30] J. J. Rojas, Y. Takashi, and M. Cho, "A lean satellite electrical power system with direct energy transfer and bus voltage regulation based on a bi-directional buck converter," *Aerospace*, vol. 7, no. 7, p. 94, Jul. 2020.

[31] A. Vobornik, I. Vertat, and R. Linhart, "Experimental electric power system for small satellites with independent supply channels," in *Proc. Int. Conf. Appl. Electron. (AE)*, Sep. 2018, pp. 1–7.

[32] H. Aung, J. J. Soon, S. T. Goh, J. M. Lew, and K.-S. Low, "Battery management system with state-of-charge and opportunistic state-of-health for a miniaturized satellite," *IEEE Trans. Aerosp. Electron. Syst.*, vol. 56, no. 4, pp. 2978–2989, Aug. 2020.

[33] K. B. Chin, E. J. Brandon, R. V. Bugga, M. C. Smart, S. C. Jones, F. C. Krause, W. C. West, and G. G. Bolotin, "Energy storage technologies for small satellite applications," *Proc. IEEE*, vol. 106, no. 3, pp. 419–428, Mar. 2018.

[34] Y.-K. Chen, Y.-C. Lai, W.-C. Lu, and A. Lin, "Design and implementation of high reliability electrical power system for 2U NutSat," *IEEE Trans. Aerosp. Electron. Syst.*, vol. 57, no. 1, pp. 614–622, Feb. 2021.

[35] J. Gonzalez-Llorente, A. A. Lidtke, K. Hatanaka, R. Kawauchi, and K.-I. Okuyama, "Solar module integrated converters as power generator in small spacecrafts: Design and verification approach," *Aerospace*, vol. 6, no. 5, p. 61, May 2019.

[36] A. Ali, S. A. Khan, M. U. Khan, H. Ali, M. Rizwan Mughal, and J. Praks, "Design of modular power management and attitude control subsystems for a microsatellite," *Int. J. Aerosp. Eng.*, vol. 2018, pp. 1–13, Dec. 2018.

[37] T. M. Lim, A. M. Cramer, J. E. Lumpp, and S. A. Rawashdeh, "A modular electrical power system architecture for small spacecraft," *IEEE Trans. Aerosp. Electron. Syst.*, vol. 54, no. 4, pp. 1832–1849, Aug. 2018.

[38] A. Edpuganti, V. Khadkikar, M. S. Elmoursi, and H. Zeineldin, "A novel multiport converter interface for solar panels of CubeSat," *IEEE Trans. Power Electron.*, pp. 1–15, 2021.

[39] A. J. Ali, M. Khalily, A. Sattarzadeh, A. Massoud, M. O. Hasna, T. Khattab, O. Yurduseven, and R. Tafazolli, "Power budgeting of LEO satellites: An electrical power system design for 5G missions," *IEEE Access*, vol. 9, pp. 113258–113269, 2021.

[40] G. Farahani and M. Taherbaneh, "Extracting best reliable scheme for electrical power subsystem (EPS) of satellite," in *Proc. 5th Int. Conf. Recent Adv. Space Technol. (RAST)*, Jun. 2011, pp. 532–537.

[41] O. Shekoofa and E. Kosari, "Comparing the topologies of satellite electrical power subsystem based on system level specifications," in *Proc. 6th Int. Conf. Recent Adv. Space Technol. (RAST)*, Jun. 2013, pp. 671–675.

[42] L. K. Slongo, S. V. Martínez, B. V. B. Eiterer, and E. A. Bezerra, "Nanosatellite electrical power system architectures: Models, simulations, and tests," *Int. J. Circuit Theory Appl.*, vol. 48, no. 12, pp. 2153–2189, Dec. 2020.

[43] A. Edpuganti, V. Khadkikar, H. Zeineldin, M. S. E. Moursi, and M. Al Hosani, "Comparison of peak power tracking based electric power system architectures for CubeSats," *IEEE Trans. Ind. Appl.*, vol. 57, no. 3, pp. 2758–2768, May 2021.

[44] A. Edpuganti, V. Khadkikar, M. S. E. Moursi, H. Zeineldin, N. Al-Sayari, and K. Al Hosani, "A comprehensive review on CubeSat electrical power system architectures," *IEEE Trans. Power Electron.*, vol. 37, no. 3, pp. 3161–3177, Mar. 2022.

BAYAN HUSSEIN (Graduate Student Member, IEEE) received the B.Sc. degree (Hons.) in electrical engineering from Qatar University, in 2020, where she is currently pursuing the M.Sc. degree in electrical engineering. She was a Research Assistant in a funded project addressing the development of fast electric vehicle battery chargers. Her research interests include power electronics, renewable energy, and power quality.

AHMED M. MASSOUD (Senior Member, IEEE) received the B.Sc. (Hons.) and M.Sc. degrees in electrical engineering from Alexandria University, Egypt, in 1997 and 2000, respectively, and the Ph.D. degree in electrical engineering from Heriot-Watt University, Edinburgh, U.K., in 2004. He is currently the Associate Dean for Research and Graduate Studies at the College of Engineering, Qatar University, Qatar, and a Professor at the Department of Electrical Engineering, College of Engineering, Qatar University. He supervised several M.Sc. and Ph.D. students at Qatar University. He has been awarded several research grants addressing research areas, such as energy storage systems, renewable energy sources, HVDC systems, electric vehicles, pulsed power applications, and power electronics for aerospace applications. He holds 12 U.S. patents. He published more than 130 journal articles in the fields of power electronics, energy conversion, and power quality. His research interests include power electronics, energy conversion, renewable energy, and power quality.

TAMER KHATTAB (Senior Member, IEEE) received the B.Sc. and M.Sc. degrees in electronics and communications engineering from Cairo University, Giza, Egypt, and the Ph.D. degree in electrical and computer engineering from The University of British Columbia (UBC), Vancouver, BC, Canada, in 2007. From 1994 to 1999, he was with IBM WTC, Giza, as a Development Team Member, and then as a Development Team Lead. From 2000 to 2003, he was with Nokia (formerly Alcatel Canada Inc.), Burnaby, BC, Canada, as a Senior Member of the Technical Staff. From 2006 to 2007, he was a Postdoctoral Fellow with The University of British Columbia, where he was involved in prototyping advanced Gbits/s wireless LAN baseband transceivers. He joined Qatar University (QU), in 2007, where he is currently a Professor of electrical engineering. In addition to more than 150 high-profile academic journals and conference publications, he has several published and pending patents. His research interests include physical layer security techniques, information-theoretic aspects of communication systems, radar and RF sensing techniques, and optical communication. He is a Senior Member of the Technical Staff with Qatar Mobility Innovation Center (QMIC), a Research and Development Center owned by QU and funded by Qatar Science and Technology Park (QSTP).

• • •